Phase segmentation in 3D X-ray images of unsaturated granular materials

Conference Paper · January 2013

CITATIONS
5

READS
430

6 authors, including:

Ghonwa Khaddour
General Commission for Scientific Agricultural Research
8 PUBLICATIONS **68** CITATIONS
SEE PROFILE

Mir Amid Hashemi
University of Nottingham
18 PUBLICATIONS **87** CITATIONS
SEE PROFILE

Simon Salager
Grenoble Institute of Technology
37 PUBLICATIONS **380** CITATIONS
SEE PROFILE

Jacques Jean Marie Desrues
French National Centre for Scientific Research
134 PUBLICATIONS **3,881** CITATIONS
SEE PROFILE

Phase segmentation in 3D X-ray images of unsaturated granular materials

Ghonwa KHADDOUR[1], Amid HASHEMI[2], Simon SALAGER[1], Jacques DESRUES[1], Thierry Jacques MASSART[2] and Bertrand FRANCOIS[2]

1Grenoble-INP, UJF-Grenoble 1, CNRS UMR 5521, 3SR Lab, Grenoble F-38041, France. E-Mail: simon.salager@3sr-grenoble.fr

2ULB, avenue F.D. Roosevelt 50, 1050 Bruxelles, Belgium. E-Mail: Bertrand.francois@ulb.ac.be

A b s t r a c t

The recent implementations of X-ray computed tomography, to analyze different responses and behaviours of various soils, are based on full-field measurements allowing to obtain morphological information at different scales. With the huge volume of details available from this technique it has become important to develop numerical key tools that allow to treat X-ray images with more analytical view, and automate the process of identification of all the present elements. In this study, a developed code of segmentation is presented, in order to extract the maximum possible information, that allow to investigate porosity and degree of saturation, at grain scale, through the study of water retention behaviour (WRB) of unsaturated sand. X-ray images, of a resolution of 7.5µm, were segmented and then used to validate this code. All the interpretations associated to this method of segmentation are discussed and can be adjusted to fit any future study.

Key words: Segmentation, Unsaturated soils, X-ray Computed Tomography.

1. INTRODUCTION

Physical properties of granular materials are important to be understood and defined in many practical applications. For unsaturated soils which are widespread in nature, two of the most important physical characteristics are porosity and degree of saturation. The understanding of these physical properties at micro-scale, will allow understanding the macro scale heterogeneity of the soil. The effect of these two properties, for partially saturated granular media, can be tracked clearly through water retention behaviour [6], [13], which can be represented by water retention curve (WRC). WRC expresses water content or degree of saturation as a function of suction. However, macro-structural and late micro-structural analysis had not provided thorough insight into the different characteristics and mechanisms of the soil.

From this point, it was needed to develop techniques and tools that allow the characterization of soils using X-ray computed tomography at grain scale. The objective of this paper is to study the local distribution of water in a sand specimen at the particle scale through X-Ray Computed Tomography images. To do so, the images must be analysed and the different phases (gas, liquid, solid) must be distinghished through an appropriate segmentation technique.

This paper presents a new code, that simplifies the process of segmentation of the three media considered in unsaturated soils (air, water and grain). This will help to define both porosity and degree of saturation at grain scale. Subsequently global macroscopic responses can be deduced and built from the local microscopic resulted responses of these soils. The paper is divided into several sections. After the introduction, a thorough description of the experimental set up is detailed in the second section. The third section is dedicated to image processing and analysis. Section four is preserved for the results with a quantitative interpretation. Lastly, a short conclusion is given to summarize the results that have been obtained.

2. EXPERIMENTAL SETUP

2.1. Material

This study was conducted on Hostun sand. The chemical components of this sand consist of high siliceous amount (SiO2 > 98%). The grain shape varies from angular to sub-angular. The WRB of this sand is characterized through its main drying path experimentally presented in Fig (1), [7].

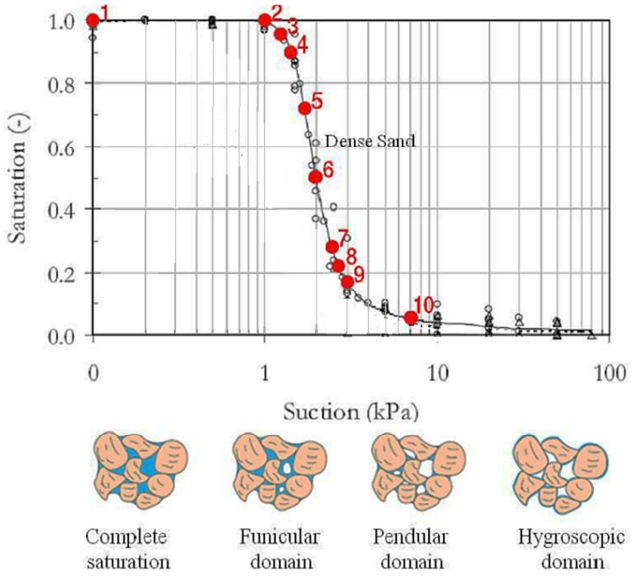

Fig. 1. Main drying path of Hostun sand. The best fit [3], and the experimental path [7].

In this reference WRC, an air-entry value of approximately 1.4 kPa was found. After reaching the air-entry value, water content decreases along a narrow range of suction. The de-saturation zone (or transition zone) is between 1.4 kPa and 2.8 kPa (water content difference of 18.5%). Therefore, it is important to apply the suction precisely, which is accomplished by using tensiometry method.
In order to analyse the microphysics behind this behaviour, different points of interest were a priori selected in this curve (a given pair of values, suction / degree of saturation) where X-Ray CT were to be performed. Attention was focused in the main drainage curve during this study and ten points (scans) were performed in it. The selected values would allow having images in all the different water retention domains (Full saturation, Funicular domain/quasi-saturation, Pendular domain/partial saturation and finally Hygroscopic domain/residual saturation). Table (1) shows the experimental program followed in this work, the corresponding points in the reference water retention curve, the suction applied and expected degree of saturation values.

Table (1) Detailed experimental program.

Point	1	2	3	4	5	6	7	8	9	10
Suction (kPa)	0	1	1.2	1.4	1.8	2	2.2	2.5	3	7
Expected Sr %	100%	99.2%	97.7%	94.6%	71.5%	46.2%	39.2%	28.8%	16.5%	5.4%

2.2. The cell and sampling technique

The need of high resolution images imposed a relatively small size of sample, which was a cylinder of 1 cm diameter and 1 cm high. The cell was built of acrylic fabric and it was designed in order to be compatible with the X-ray tomography technique. Fig (2) shows the details of the cell apparatus.

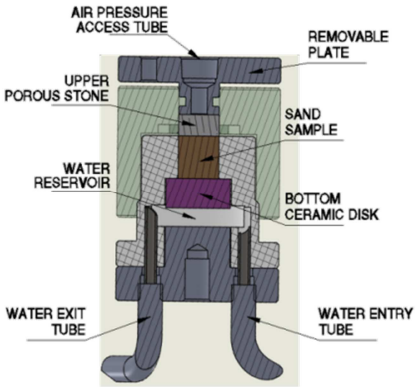

Fig. 2. The cell, and its component parts, [13].

Since the experiment begins with a completely saturated state, all the voids in the sample have to be completely saturated with water before starting the experiment. The sample was prepared with having the cell completely submerged under water, after that the sand was simply dropped little by little from a certain height under water using a small spoon, see Fig (3). All the water used in this work was de-mineralised and de-aired for 24 hours using a magnetic stirring heater.

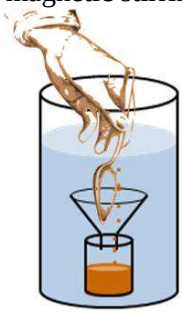

Fig. 4. X-ray CT scanner at Laboratoire 3S-R, inside of the cabin.

2.3. Suction application and the experimental protocol

In this study, a pressure controller device allows the application of a positive air pressure that increases the suction by the tensiometry method. The cell was then placed inside the X-Ray cabinet, see Fig (4), where all the arrangement is already prepared, and connected to the system paying special attention not to incorporate air in any part of it.

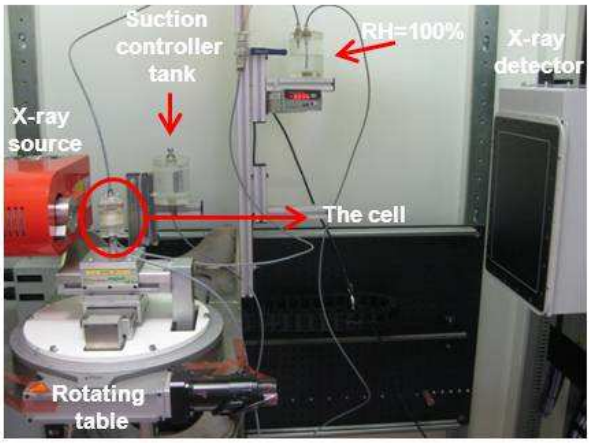

Fig. 4. X-ray CT scanner at Laboratoire 3S-R, inside of the cabin.

The first scan corresponds to a fully saturated sample. Then the first suction value was applied by moving down the tank in the scale rule “tensiometry”. In order to reach a stable condition with no flow

of water, the cell was left for the needed time. This time was taken from experiments [7] and it was ranged between 2and 3 days. Fig (5) shows a sketch of the arrangement.

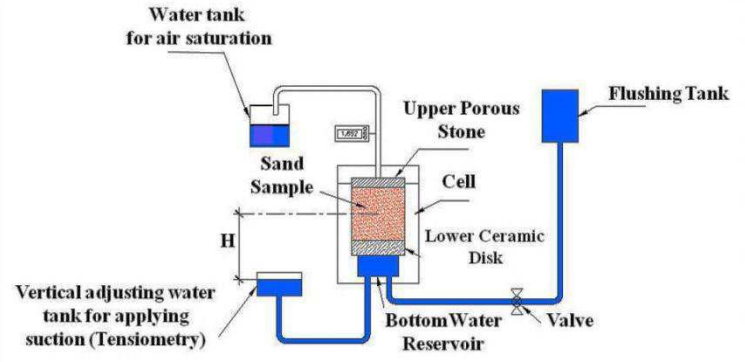

Fig. 5. Sketch of the arrangement used in the present work, [13].

Finally, after the last scan, the cell was carefully opened, the whole volume of sand recovered and dried in an oven for 24 hours and then weighed. The precise weight of the solid phase in the sample is needed to compare this value to the value resulted from segmentation process.

2.4. X-ray tomography

X-ray micro-CT is a non-destructive, 3D high resolution imaging method that allows the internal structure of objects to be investigated. The use of X-ray imaging here is demonstrated for visualizing and quantifying water distribution in partially saturated granular porous media. Because of the unique difference in the attenuation coefficient of water, sand, and air, a significant contrast for the three phases is observed in an electron transmission image, and a quantitative analysis provides detailed information on the arrangement and distribution of particles, voids, and water. The experiments in this study are performed at 3SR LAB at (UJF). The acquisition of images and control is carried out by means of the software RX-act developed by RX solutions (Annecy, France). The resolution acquired for the resulting images was near the highest the device allows (7.5 μm).

3. IMAGE PROCESSING AND ANALYSIS

After image acquisition, the set of images obtained from different angles (called radiograms) have to be processed in order to reconstruct the entire scanned volume. Two different softwares were used in this work. Real Image Viewer 2.4.2 and DigiCT 2.4.2 developed by Digisens (Lyon, France). The first one is used to correct the displacement of the radiograms produced by temperature variation during acquisition and the later to do the reconstruction itself (feldkamp filtered back projection). The reconstruction of the images is done between two acquisitions. Subsequently, the reconstructed slices are visualised and analysed by the images processing software Image J. After that the images have been trinarized using a Matlab code based on region growing type segmentation [4].

3.1. Image segmentation

The main objective of image segmenting is partitioning of the image into regions or objects of interest. It consists of labelling each voxel according to its intensity value relative to a reference parameter known as the intensity threshold. The distribution of the number of voxels as a function of their intensity level, known as the histogram, is a widely used tool in image processing. For the images considered in this study, there are three main phases, the solid phase formed by voxels representing the particles, the liquid phase (water) and the gas phase (air) which are respectively associated with voxels representing air and water. For the tomographic images obtained by absorption contrast, low-density phase has lower intensity values than high-density material (solid grains) and so air voxels look darker than the solid voxels. Water has an intermediate gray level. Therefore the typical histogram for these images has three peaks/values, Fig (6), two filled voids, water and air, and one for the grain particles.

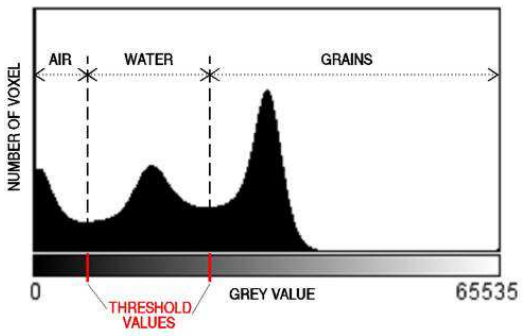

Fig. 6. Histogram peaks for grain, water and air.

T The number of voxels located in the gap between two peaks can be associated with the partial volume effect caused by voxels whose intensity is an average of the attenuation of two materials in the soil samples (soil and water, water and air, sand and air) due to the finite resolution of the images. On other hand, the noise caused by voxels with random intensity (overlapping between grain/water or water/air histograms), can contribute to increase the number of voxels located between the peaks of the histogram.

3.2. Segmentation numerical code

Thresholding is the simplest method of image segmentation. The key parameter in the thresholding process is the choice of the threshold value for each phase (air/water/grain). Different methods exist for finding the threshold value, such as stochastic watershed [1], watershed [2], split-and-merge [5], level-set [8], edge detection [9], statistical region merging [10], anisotropic diffusion [11], and region-growing [12]. These approaches were well adapted and efficient when few objects have to be identified. For granular materials, the number of objects can be very high and its segmentation often require excessive computational time. Using human eye, it seems possible to distinguish the regions occupied by each phase. However, due to the large number of particles, it could be hard to visualize each phase clearly. Therefore numerical automated technique must be used to extract phases boundaries in a fast, easy and systematic procedure. Consequently, a more sophisticated physical approach was developed and implemented. It is a region-growing type segmentation, that allows performing a simultaneous segmentation of 3-phase tomographic images of a granular material. The code can be summarized into four steps:

- partial thresholding.
- partial volume effect filtering.
- simultaneous phase growing which constitutes the main step.
- interface filling.

The procedure is applied on 3D X-ray 8-bits [(0-256) gray level range] reconstructed images.

3.2.1.Partial thresholding

The first step is to set four different (partial) thresholds. On one hand, these partial thresholds will define the regions, where it is sure that the phase are present. Meaning, for sand partial threshold, the region where only sand exists surely, will be defined. On other hand, these partial thresholds, will exert a ‘barrier’ against other phases preventing them from growing towards its direction. These thresholds are chosen as the peak values for both sand and air histograms, defining by that 50% of both Gaussian curves. Thus for 8bits image histogram, the range between [zero, air thresholds] and [grain thresholds, 256] is determined and not to be discussed in the following steps, see Fig (7).

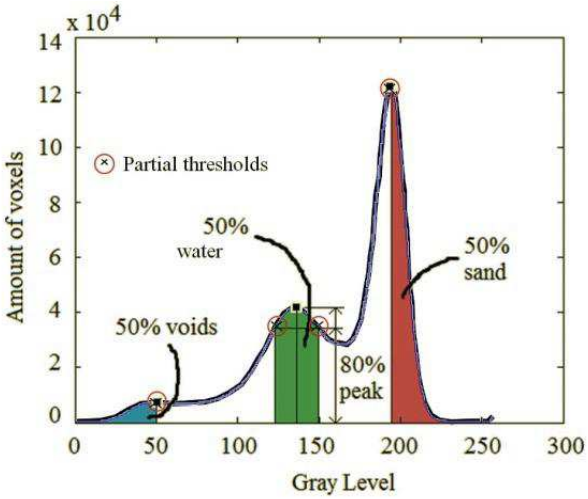

Fig. 7. Partial thresholds definition, [4].

For the middle histogram curve (water curve), a range centred at the peak of water curve and extend 25% to the left and to the right of the peak is considered. This is achieved by locating where the Gaussian curve of this phase decreases to 80% of its peak, see Fig (7). Consequently, four partial thresholds [$P_{air} < P_{1\text{-}water} < P_{2\text{-}water} < P_{grain}$] are determined, and around of 50% of each phase is being decided to be either air or water or grain. But, as already explained, PVE appears as gray levels located between air and grain Gaussian curves as a consequence of image resolution. This effect takes place when grain/water or water/air phases are taken into account into one voxel. This voxel is then representative of both phases showing an intermediate gray value corresponding to a balanced average of the gray levels of two distinct objects. Therefore, the gray value of PVE depends on the percentage of each phase in the voxel. Thresholding the image by selecting the middle phase, will also select voxels located at the interface between the two others due to PVE (Fig (9)). Thus, this limitation of the first step is to be corrected in the second step.

3.2.2.Partial volume effect filtering

The surroundings of a voxel not influenced by PVE is made of voxels having close gray values. A spherical selection around this voxel will result in the histogram in an approximate Gaussian curve centred on the middle phase gray value. Conversely, the surrounding of a voxel from PVE mostly contains voxels from both air and grain gray phases, Fig (8).

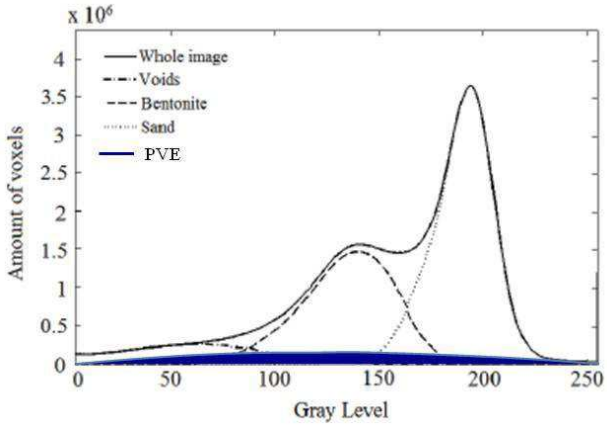

Fig. 8. Partial volume effect histogram, [3].

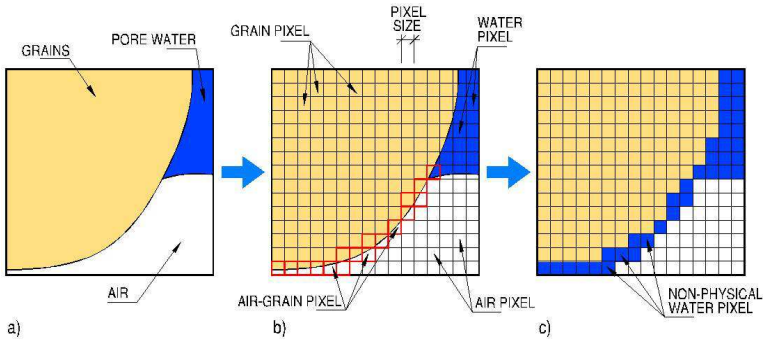

Fig. 9. Partial volume effect at the interface. a) Reconstructed images of grays. b) Corresponding pixels. c) Trinarized image with wrong assigned values.

In this paper, an optimal radius of 2 voxels is used for this spherical selection. The choice of sphere radius is a rational process, governed by the fact that, if a radius of 1 voxel (representing the 6 nearest neighbours) was chosen, this would not give sufficient information for the variance calculation, while choosing a larger radius would not consider the direct neighbourhood of the voxel. The standard deviation of the voxels surrounding each voxel (after excluding all the voxels defined from the first step) can be used to separate the real middle phase voxels from PVE voxels. These voxel with high standard deviation (PVE voxels) are then excluded by using a threshold filtering of the standard deviation. The threshold is taken at the inflexion point on the histogram, Fig (9).

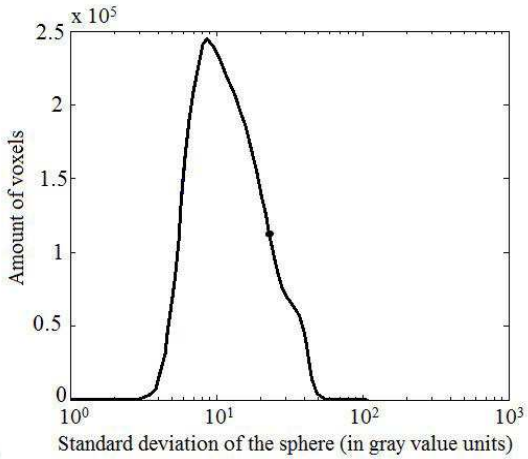

Fig. 10. Standard deviation threshold, [4].

This adaptation shows a good efficiency by filtering most of the voxels located at the interface between voids and sand particles.

3.2.3.Simultaneous phase growing

The selection of 50% of each phase by doing a partial threshold will represent on the 3D image a group of voxels selected homogeneously in each phase (due to the effect of Gaussian noise). Consequently, the neighbours of each partial threshold represents practically the other half of the phase. Since the image is three-dimensional, there are six neighbours next to each voxel considered. As more neighbours are selected, the image is practically filled. At this stage, these remaining voxels represent the interface between different phases. This interface is not assigned to any phase because it can belong to one of the neighbour phases but this problem will be solved afterwards. At this stage, there is still a probability for other phase voxels, water for example, to be mistakenly selected for the sand phase. Indeed, the first phase that ‘reaches’ a new voxel incorporates it, but the phases do not ‘see’ where they grow. Consequently, there is a potential for overgrowing in some areas of the image.

This phenomenon may be limited by choosing adequate partial thresholds (at the first step) of the process, whereas the initial phases will prevent other phases from growing in their neighbourhood. To avoid for each phase to grow in extreme gray values, a 'tolerance threshold' is therefore chosen [T_{air}, $T_{1\text{-water}}$, $T_{2\text{-water}}$ and T_{grain}], for each phase, to exclude the gray values where the phase is assumed not to be present. These exclusions can be determined by setting the gray value from which the Gaussian curve of each phase can be neglected. The existence of PVE must also be considered here. After PVE filtering, some voxels of middle region of the total histogram (belonging to air or grain phase in reality) are not taken into account inside the partial threshold. The tolerance thresholds for the air and grain have to be large enough to consider these voxels. Consequently, it is recommended to define the tolerance thresholds of air and grain as equal. Fig (11) summarizes the choice of the partial and tolerance thresholds in this procedure. From the figure it could be seen that it is enough to define the partial thresholds and then to set the tolerance thresholds equal to some partial thresholds, e.g. $T_{air}=P_{1\text{-water}}$, $T_{grain}=P_{2\text{-water}}$, $T_{1\text{-water}}=P_{air}$ and $T_{2\text{-water}}=P_{grain}$

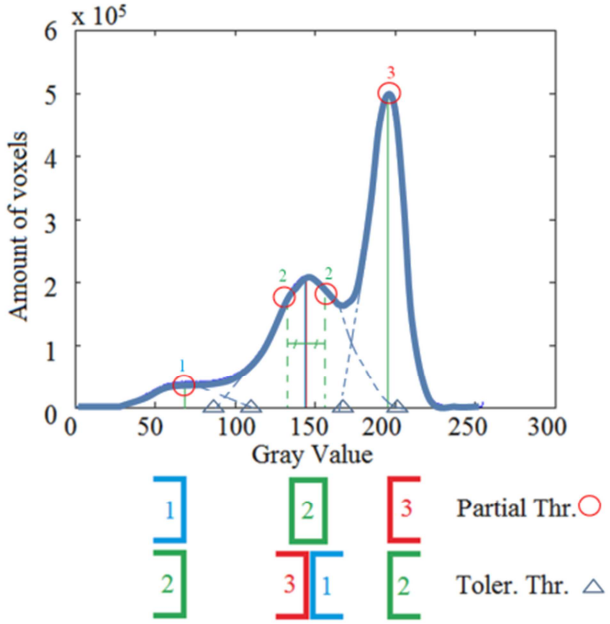

Fig. 11. Definition of tolerance thresholds from partial thresholds, [4].

3.2.4. Interface filling

At the end of the phase growing step, some of the voxels remain at the interfaces. The final step of the procedure is to determine the phases to which, the voxels of the interface are belonging. For each voxel at the interface, another sphere selects the surrounding voxels. The most present phase inside the sphere will determine the phase segmentation. If two phases are equal in amount in the sphere, the considered voxels remain undecided. This procedure is repeated and, usually after 4 repetitions, the most of the voxels have been filled. At the end, the remaining voxels are defined with a simple threshold method and the phases are attributed as a function of the voxels gray level.

4. RESULTS

4.1. Trinarisation results

Reconstructed X-ray images of Hostun sand sampleconsisting in 1500 horizontal slices were trinarized using using the developed code. Fig (12) shows a group of results, present horizontally and vertically trinarized slices for different values of suction (s= 0, 1, 1.2, 1.4, 1.8, 2, 2.2, 2.5, 3 and 7 kPa) and different water domains of WRC.

s=2 kPa	s=1.8 kPa	s=1.4 kPa	s=1.2 kPa	s=1 kPa	s=0 kPa	
Pendular Zone				Saturated Zone		
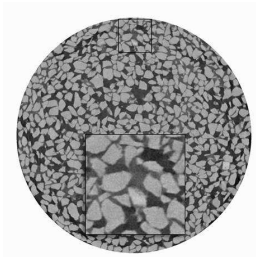	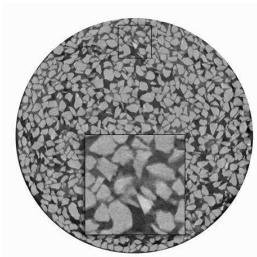	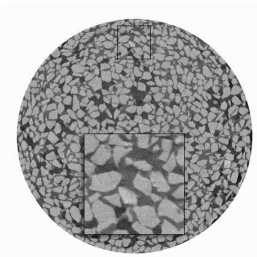	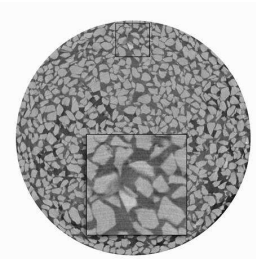	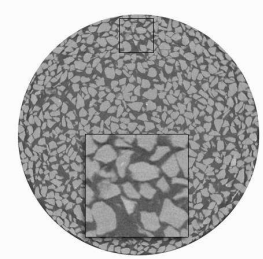	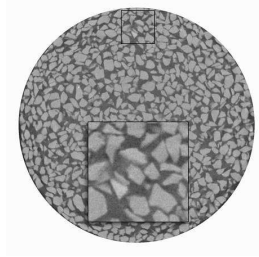	(a)
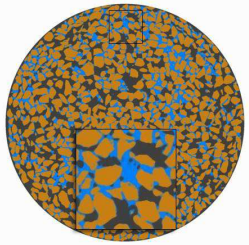	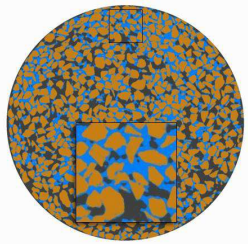	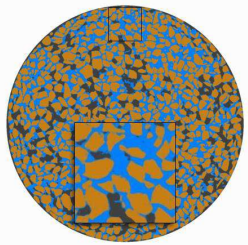	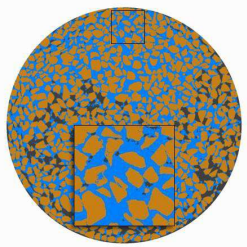	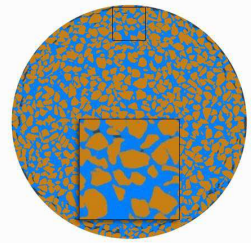	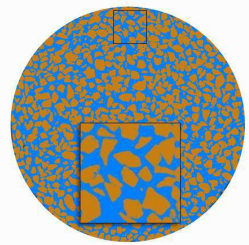	(b)
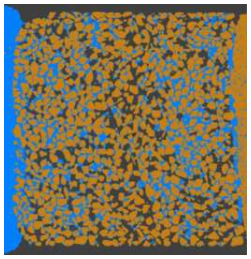	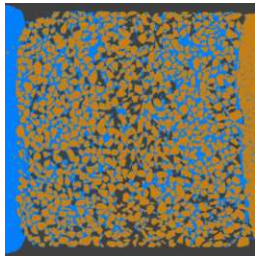	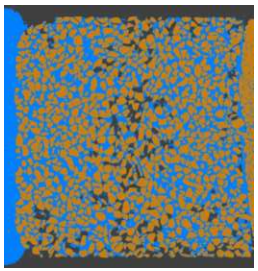	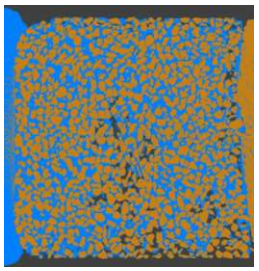	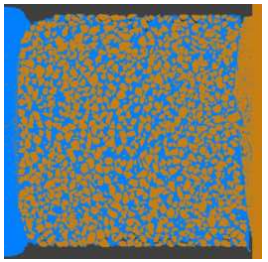	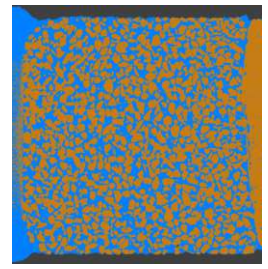	(c)

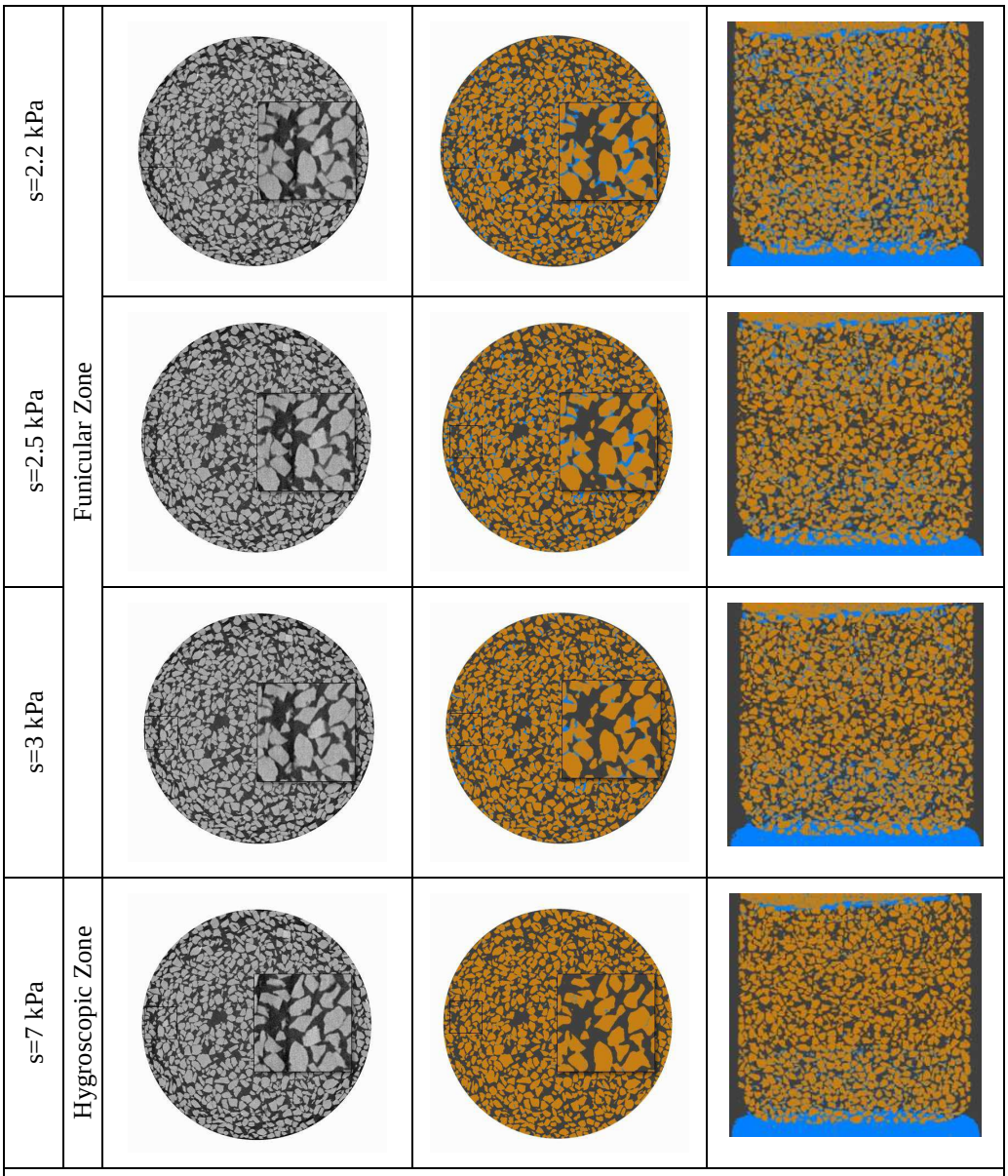

Fig. 12. Trinarized images for Suction values equal to 1, 1.2, 1.4, 1.8, 2, 2.2, 2.5, 3 and 7 kPa for Horizontal slice N° 800. a) Reconstructed horizontal slices b) Trinarized horizontal slices. c) Trinarized vertical slices at the centre of the sample.

The results show that, for the saturated case, s=0kPa, no air presence could be noticed, and the vertical section shows that water fills all the voids inside the sample. Once suction is applied (s=1kPa), air starts to get inside the sample from the edges as it is shown in the vertical section. This can be due to the weak surface connection between the sample and the cell. Increasing the value of suction (s=1.2 kPa), the net of connected empty voids starts to be formed, leading to conclude, that air entry value is between (s=1kPa) and (s=1.2kPa). Under that range of suction, air empties the bigger connected voids first before the small ones, soil behaviour of water retention in the pendular domain can be justified through the middle part. This middle area of the sample lost water gradually with increasing negative pressure. In the funicular domain, water starts to drain out of the sample, leaving traces that could be hardly seen by the human eyes, until reaching the hygroscopic domain where water can be seen only on/near the surface of the grains, governed by surface tension.

The reasons causing water to flow out from the middle area could be due to big connected voids, which can lead to ink-bottle effect, while for the upper and lower area of the sample, where narrow small voids exist, water may be retained through capillary effect. The trinarized volumes, will allow now the estimation of the physical parameters of soil digitally and in the whole sample field. For fu-

ture studies, the local porosity and degree of saturation can be analyzed and calculated in the entire sample using these volumes, [13].

4.2. Discussion

4.2.1.Macroscopic (Global) porosity and degree of saturation estimation

In order to have the ability to evaluate the results of the developed segmentation code, this step of estimation was a helpful validation tool. Macroscopic porosity was calculated in two different ways. The first method came by porosity definition its self, by dividing the volume of voids over the total considered volume, $n=V_v/V_t$ .The weight of the dry sand in the sample (solid phase) is known since it was perfectly measured after the last scan. The volume of grains is obtainable knowing its weight and the density of solid grains (V_s=(1.16 g)/(2.65g/cm3)=0.4377 cm3 for this study). Having the approximate volume of the cell V_t=0.785 cm3 (cylinder of 1 cm diameter and 1 cm height), the global porosity should be around: $n=V_v/V_t=(V_t–V_s)/V_t$=44%.

The second method to calculate porosity is by using the trinarized images. The 8-bits resulted trinarized images are of three gray values, zero for air, 128 for water and 255 for grain. The histogram of this images will give three values correspond to the number of pixels that represent air (P_a), water (P_w) and grains (P_g). Through the number of pixels representing each phase, both macroscopic porosity and degree of saturation were calculated as following:

$$\text{Porosity} = \text{n} = \frac{\text{total volume of pixels} - \text{grain pixels}}{\text{total volume of pixels}} = \frac{(\text{Pg} + \text{Pw} + \text{Pa}) - \text{Pg}}{\text{Pg} + \text{Pw} + \text{Pa}}$$

$$\text{Degree of saturation} = \text{Sr} = \frac{\text{Pw}/(\text{Pg} + \text{Pw} + \text{Pa})}{\text{n}}$$

Table (2). Macroscopic computations of porosity and degree of saturation.

Scan (kpa)	Air (Pa)	Water (Pw)	Grain (Pg)	Porosity (n)	Degree of saturation (Sr)	Expected Sr%
Sat	0.1×10^7	50×10^7	70×10^7	0.42	0.997	1
1	0.2×10^7	56×10^7	72×10^7	0.44	0.995	0.992
1,2	12×10^7	51×10^7	83×10^7	0.44	0.806	0.977
1,4	10×10^7	43×10^7	65×10^7	0.45	0.798	0.946
1,8	30×10^7	39×10^7	81×10^7	0.44	0.632	0.715
2	30×10^7	26×10^7	72×10^7	0.44	0.469	0.462
2.2	43×10^7	13×10^7	74×10^7	0.43	0.233	0.392
2.5	46×10^7	9×10^7	74×10^7	0.43	0.176	0.288
3	52×10^7	9×10^7	81×10^7	0.43	0.147	0.165
7	51×10^7	3×10^7	73×10^7	0.43	0.067	0.054

By comparing these results to the one computed at the beginning (n=44%.), trinarisation method can be evaluated as well adapted , with an accuracy equal to 1%. For the degree of saturation, from its definition (dividing water volume over voids volume, $Sr=V_w/V_v$), local estimation cannot be done since water volume for different values of suction is not known. Still local measurements to define the number of pixels representing water, can easily be found as seen in Table (2). These values can be compared (for a comprehensive understanding) to the expected extracted values from experimental WRC [7] for Hostun sand, knowing that the refrence experiement has been conducted for a different density and porosity of Hostun sand, which will give different values of degree of saturation than the one expected for this study.

5. SUMMARY AND CONCLUSION

An experimental campaign was set in the framework of the micro-scale analysis of unsaturated sand and its water retention behaviour through X-Ray CT. A ‘step-by-step’ protocol to obtain reconstructed volumes of sufficient quality, where the three phases of the sample can be clearly distinguished was also presented. A numerical developed technique of segmentation was discussed and applied in details. The trinarized images, where the phases have been recognized and separated, helped with the visualization and characterization of homogeneity of the sample and water distribution. A qualitative interpretation of the resulting images has been done focused first, on the air entry value and water retention domains. Later, the attention was directed to the porosity and degree of saturation. A quantitative analysis was done by the estimation of soil variables. However, both the experimental technique and the image processing can be improved. The use of high quality images (small pixel size, clear distinct gray values for different phase pixels, segmentation parameters etc.) is a good starting point for reducing errors in any future analysis.

References

[1] Angulo J., Jeulin D.(2007). Stochastic watershed segmentation. In International Symposium on Mathematical Morphology, pages 265{276, 2007.

[2] Beucher S., Meyer F.(1993). The morphological approach to segmentation: the watershed transformation. In Dougherty ER, editor, Mathematical Morphology in Image Processing, pages 433{481, 1993.

[3] Fredlund, D.G., and Xing, A., (1994). Equations for the soil-water characteristic curve, Canadian Geotecnical Journal.,31: 521-532.

[4] Hashemi M. A., Khaddour G., François B., Massart T. J., Salager S.(2013). A tomographic imagery segmentation methodology of multi-phase granular materials based on simultaneous region growing. January 8, 2013. Manuscript sumbitted for publication.

[5] Horowitz SL., Pavlidis T.(1974). Picture segmentation by a directed split and- merge procedure. Proceedings of the 2nd International Joint Conference on Pattern Recognition, Copenhagen, Denmark, pages 424{433, 1974.

[6] Khaddour G., Andò E., Salager S., Bésuelle P., Viggiani G., Hall S., Desrues J.(2013). Application of X-ray tomography to the characterisation of grain-scale mechanisms in sand. Multiphysical Testing of Soils and Shales , Springer Series in Geomechanics and Geoengineering, 2013, Part 4, 195-200, DOI: 10.1007/978-3-642-32492-5_23.

[7] Lins, I.(2009). Hydro-mechanical properties of partially saturated sand. PhD Thesis. University Bochum, Germany.

[8] Malladi R., Sethian JA., Vermuri BC.(1993). A topology independent shape modelling scheme. In Proceedings of SPIE Conference on Geometric Methods in Computer Vision II, volume 2031, pages 246{258, San Diego,CA, 1993.

[9] Marr D and Hildreth E. Theory of edge detection. Proceedings of the Royal Society of London Series B-Biological Sciences, 207:187{217,1980.

[10] Nock R., Nielsen F.(2004). Statistical region merging. IEEE transactions on pattern analysis and machine intelligence, 26(11):1452{1458, 2004.

[11] Perona P.(1990). Scale-space and edge detection using anisotropic diffusion. IEEE Transactions Pattern Analysis and Machine Intelligence, 12(7):629{639, 1990.

[12] Phan DL., Xu C., Price J.(2000). A survey of current methods in medical image segmentation. Annual Review of Biomedical Engineering, 2:315{338, 2000.

[13] Riedel I., Andò E., Salager S., Bésuelle P., Viggiani G. (2012). Water retention behaviour explored by X-ray CT analysis. Springer Series in Unsaturated Soils: Research and Applications 2012, Part 1, 81-88, DOI: 10.1007/978-3-642-31116-1_11.